Surface Science 616 (2013) 44–50

Contents lists available at SciVerse ScienceDirect

Surface Science

journal homepage: www.elsevier.com/locate/susc

Peculiar diffusion of C_{60} on In-adsorbed Si(111)$\sqrt{3} \times \sqrt{3}$-Au surface

A.V. Matetskiy [a,b], L.V. Bondarenko [a,b], D.V. Gruznev [a,b], A.V. Zotov [a,b,c], A.A. Saranin [a,b,*], J.P. Chou [d], C.R. Hsing [d], C.M. Wei [d], Y.L. Wang [d]

[a] Institute of Automation and Control Processes, 5 Radio Street, 690041 Vladivostok, Russia
[b] School of Natural Sciences, Far Eastern Federal University, 690950 Vladivostok, Russia
[c] Department of Electronics, Vladivostok State University of Economics and Service, 690600 Vladivostok, Russia
[d] Institute of Atomic and Molecular Sciences, Academia Sinica, P.O. Box 23-166, Taipei, Taiwan

ARTICLE INFO

Article history:
Received 9 January 2013
Accepted 19 May 2013
Available online 24 May 2013

Keywords:
Atom–solid interactions
Silicon
Fullerene
Surface diffusion
Scanning tunneling microscopy
First-principle calculations

ABSTRACT

In-accumulated Si(111)$\sqrt{3} \times \sqrt{3}$-Au surface represents a highly-ordered homogeneous Au/Si(111) reconstruction with a two-dimensional gas of In adatoms on it. Regularities of C_{60} migration on this surface have been elucidated through analysis of C_{60} island density as a function of growth temperature and deposition rate in the framework of the rate equation theory and simulation of C_{60} migration using density-functional-theory calculations. The critical cluster size has been found to be $i = 1$ for the whole temperature range studied, from 110 to 240 K, while activation energy for C_{60} diffusion varies from (99 ± 18) meV at 110 ÷ 140 K to (370 ± 24) meV at 160 ÷ 240 K. This finding has been accounted to the peculiarity of C_{60} migration in a labyrinth built of In adatoms on the Si(111)$\sqrt{3} \times \sqrt{3}$-Au surface, namely, at low temperatures C_{60} migration is confined within the labyrinth channels, while at high temperatures C_{60} molecules possess enough thermal energy to surmount the labyrinth walls.

1. Introduction

Elucidating the regularities of atomic and molecular island formation has been a long-standing problem in surface physics and material science. Considerable efforts in this field have resulted in developing powerful theoretical approaches. In particular, the rate equation theory establishes a quantitative relationship between the island density N (which can be directly measured in the experiment as a function of deposition rate R and growth temperature T) and characteristics of the atomic processes involved in island formation, including a surface diffusion barrier of adatoms E_{diff}, a critical island size i and a binding energy E_i gained in forming the critical island [1]:

$$N \propto \left(\frac{R}{\nu_0}\right)^{i/(i+2)} \exp\left(\frac{iE_{diff} + E_i}{(i+2)k_B T}\right), \quad (1)$$

where ν_0 is the attempt frequency and k_B is the Boltzmann constant. Remind that a critical island size i is defined as one less than the number of atoms needed to form the smallest stable island. Efficiency of this classical approach (confirmed also with Monte Carlo simulations [2]) has been proved in the numerous studies on island formation in the variety of adsorbate–substrate systems [3–7]. Recently, the approach has been extended for more complicated cases (e.g., island growth mediated by formation of mobile clusters [8] or growth of compound islands [9,10]).

In recent years, self-assembly of the adsorbed molecular species into complex supramolecular structures has attracted considerable attention motivated by potential applications in molecular electronics. Fullerene C_{60} is believed to be a fascinating molecule from a nanoelectronics and nanoscience perspective. It is thought to be an ideal block for molecular devices due to its ability to accept electrons from other molecules, atoms, and surfaces [11]. Peculiarities of C_{60} island growth on the bare substrate surfaces [12–15] as well as those modified by adsorption of foreign atoms or molecules [16–21] have recently attracted a considerable interest. As for characterization of the C_{60} surface diffusion, monitoring of a single molecule migration [22,23] and evaluation of island density using the rate equation theory [14] have demonstrated their efficiency.

In this work, we employed the latter approach for characterization of C_{60} diffusion on Si(111)$\sqrt{3} \times \sqrt{3}$-Au surface. Before C_{60} deposition, the surface was modified by adsorption of ~0.14 ML of In to eliminate the domain wall network [24] characteristic of the original Au/Si(111) surface [25]. This surface has been shown to possess advanced properties of a perfect isotropic two-dimensional electron-gas system [26] with a large spin splitting of the surface state bands [27] which can be affected by adsorption of C_{60} molecules due to their acceptor-type behavior [28]. The properly prepared Si(111)$\sqrt{3} \times \sqrt{3}$ – (Au, In) surface is highly-ordered and contains extremely low density of surface defects. The presence of the 2D gas of In adatoms is its peculiar feature which

* Corresponding author at: Institute of Automation and Control Processes, 5 Radio Street, 690041 Vladivostok, Russia.
E-mail address: saranin@iacp.dvo.ru (A.A. Saranin).

0039-6028/$ – see front matter © 2013 Elsevier B.V. All rights reserved.
http://dx.doi.org/10.1016/j.susc.2013.05.011

allows to explore an interesting case of surface diffusion when two types of species, adatoms and molecules, are involved simultaneously in the diffusion process. We have found that while a critical island size $i = 1$ remains the same for the whole temperature range studied, the diffusion barrier for C_{60} is ~3.7 times greater for the "hot" surface (370 meV at 160–240 K) than for the "cold" surface (99 meV at 110–140 K). Possible origin of the phenomenon is discussed basing on the results of the density-functional-theory (DFT) calculations.

2. Experimental and calculation details

Our experiments were performed with an Omicron STM operating in an ultrahigh vacuum (~7.0×10^{-11} Torr). Atomically-clean Si(111) 7×7 surfaces were prepared in situ by flashing to 1280 °C after the samples were first outgassed at 600 °C for several hours. Gold was deposited from an Au-wrapped tungsten filament, indium from Ta crucible and C_{60} fullerenes from a resistively heated Mo crucible. For STM observations, electrochemically etched tungsten tips cleaned by in situ heating were employed.

To prepare the highly-ordered homogeneous In-adsorbed Si(111) $\sqrt{3} \times \sqrt{3}$-Au surface, the following procedure was used. First, the Si(111)-α-$\sqrt{3} \times \sqrt{3}$-Au surface [25] was formed by Au deposition at 700 °C. Then, ~0.5 ML of In was deposited onto this surface held at room temperature followed by brief (~15 s) annealing at 400 °C. The resultant surface preserves the atomic arrangement of pristine Si(111) $\sqrt{3} \times \sqrt{3}$-Au phase described by the conjugate-honeycomb chained trimer model [29–31,27]. It contains also ~0.14 ML of In left after high-temperature treatment and forming a 2D gas of adatoms [24,26].

To elucidate the experimental observations, systematic first-principle calculations based on the density functional theory (DFT) are performed. We employ the Vienna ab-initio simulation package (VASP) [32,33] with the projector augmented wave [34] pseudopotentials. In previous DFT calculations, the local density approximation [35,36] (LDA) has been shown to be able to well describe both the electronic and energetic properties of C_{60} adsorbed onto Au(111) [37,38] Ag(111) [38,39], and Ag(100) [37]. However, LDA describe the van der Waals (vdW) forces less accurately, which is important in C_{60}–metal and C_{60}–C_{60} interactions [40]. Therefore, in this work, the non-local van der Waals density functional (vdW-DF2) [41–43] method as implemented in VASP code has been employed. The Kohn–Sham wave functions are represented using a plane-wave basis set with a kinetic energy cutoff of 300 eV. The surface is simulated by a repeated slab with a $2\sqrt{3} \times 2\sqrt{3}$ lateral periodicity in which one Si + Au surface layer and four Si bi-layers are included. All atoms in the simulation model are fully relaxed except one bottom Si bi-layer is fixed at their bulk positions, and hydrogen atoms are used to passivate the Si dangling bonds at the bottom surface of the slab in the fixed positions. The vacuum region between slabs was ~17 Å. The Brillouin zone integration is performed with a $3 \times 3 \times 1$ k-point mesh which produces the well-converged results. The geometry is optimized until the total energy is converged to 10^{-4} eV. We applied the nudge elastic band (NEB) method [44] to find the energy barrier for the given diffusion pathways. NEB procedures interpolate a series of atomic configurations (so-called images) aligned in a pathway between the specific initial and final states, and then optimize these images by minimizing the total energies of the string images. In this way, the energy profile of diffusion process is obtained and the diffusion energy barrier is also revealed. In this study, we used a set of fifteen images including initial and final states to describe each diffusion pathway (except for the pathway A–B–C, where twenty-one images were used).

3. Results and discussion

Fig. 1 summarizes the results of STM observations on how the substrate temperature affects the forming C_{60} island array. Each time 0.1 ML of C_{60} was deposited onto the surface held at a given temperature after which STM observations were immediately conducted without changing the sample temperature. Hereafter, C_{60} coverage is given in the units of the completed fullerite-like (111) layer, i.e., 1 ML = 1.15×10^{14} cm^{-2}. One can see in the STM images in Fig. 1a the following typical trend: the island density decreases with growing temperature, while the island mean size consequently increases. Quantitative temperature dependence of C_{60} island number density is presented by the Arrhenius plot in Fig. 1b. One can clearly distinguish two regions which differ in slope and indicate different regimes of island nucleation on the "cold" surface (at 110–140 K) and on the "hot" surface (at 160–240 K). These regimes are characterized by effective activation energies of 33 and 123 meV, respectively.

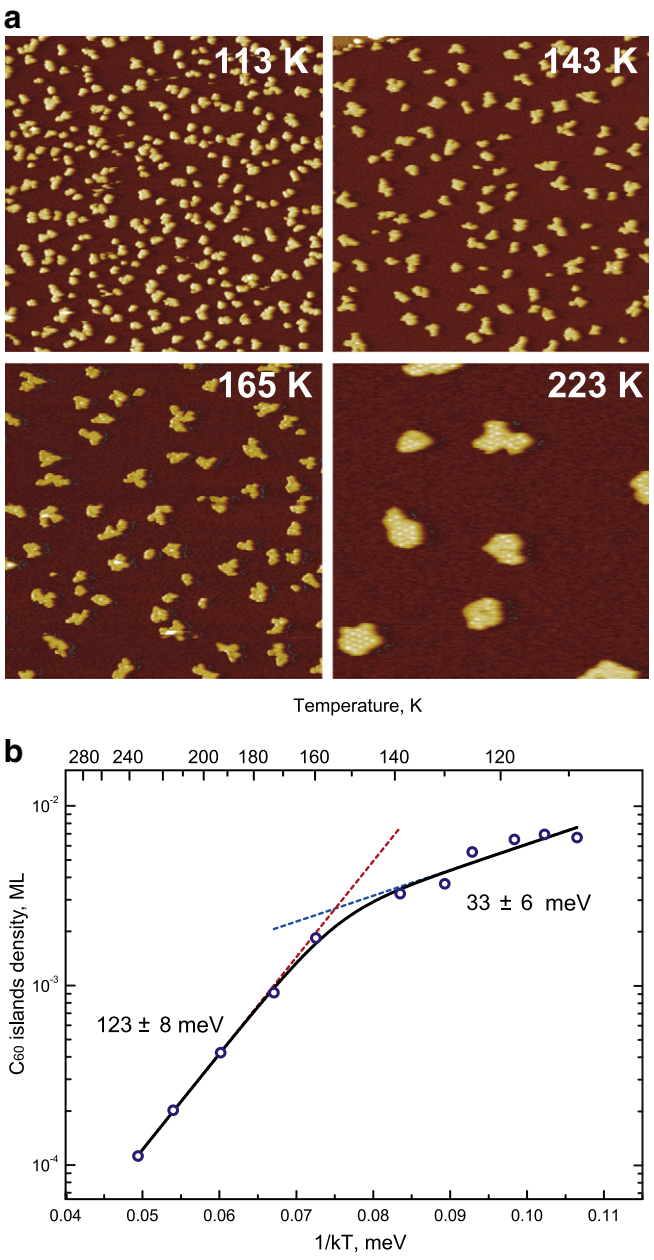

Fig. 1. (a) 200 × 200 nm^2 STM images showing C_{60} island arrays formed by depositing 0.1 ML onto Si(111)$\sqrt{3} \times \sqrt{3}$-(Au,In) surface held at various temperatures. (b) Arrhenius plot of C_{60} island number density. Dashed blue and red lines show the plots for low-temperature (110–140 K) and high-temperature (160–240 K) ranges, respectively; the sum of two exponents is shown by the black line.

To proceed further with evaluation of the diffusion parameters, one needs to establish a critical island size i. As one can see in Eq. (1), this

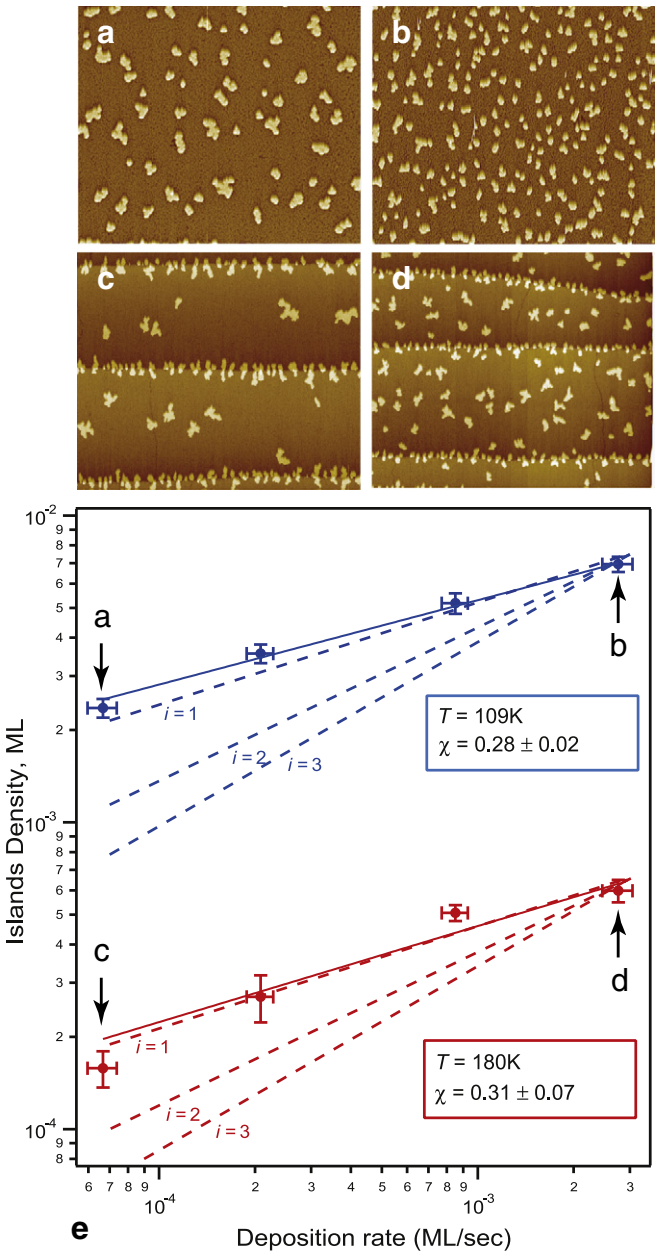

Fig. 2. Effect of C_{60} deposition rate on C_{60} island number density. (a) and (b) 170 × 142 nm^2 STM images of C_{60} island arrays formed at 109 K with C_{60} deposition rate of 7×10^{-5} and 3×10^{-3} ML/s, respectively. (c) and (d) 440 × 365 nm^2 STM images of C_{60} island arrays formed at 180 K with C_{60} deposition rate of 7×10^{-5} and 3×10^{-3} ML/s, respectively. (e) Double-logarithmic plots of C_{60} island number density versus C_{60} deposition rate for 109 and 180 K (upper and lower plots, respectively). The dashed lines show the calculated dependences for $i = 1$, 2, and 3. The experimental dots marked by characters correspond to the arrays shown in the STM images.

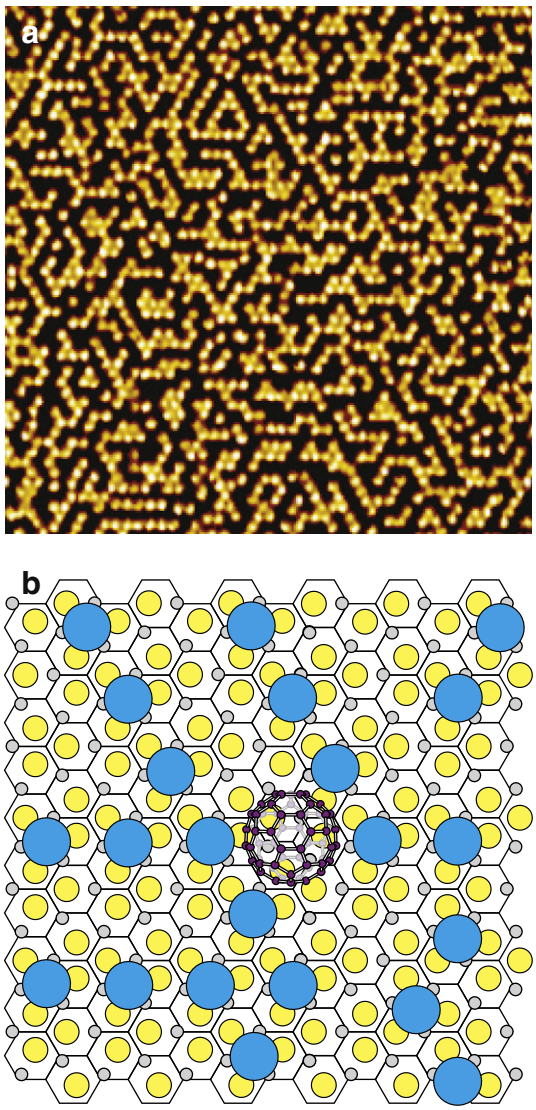

Fig. 3. (a) 27 × 27 nm^2 STM image of the (Au,In)/Si(111) surface at 110 K showing an array of immobile (frozen) In adatoms. (b) Schematic model illustrating C_{60} in the labyrinth built of In adatoms (blue circles) on Si(111)$\sqrt{3} \times \sqrt{3}$-Au CHCT surface with Au atoms shown by yellow circles and Si atoms by gray circles.

can be done by measuring the rate dependence of island density at a fixed temperature. Fig. 2 summarizes the results of evaluations conducted at two temperatures, 109 and 180 K (i.e., those corresponding to the different regimes of island nucleation). Fig. 2a and b shows 170 × 142 nm^2 STM images of C_{60} island arrays grown at 109 K with C_{60} deposition rate of 7×10^{-5} and 3×10^{-3} ML/s, respectively. Fig. 2c and d shows the same but obtained at 180 K. Note that as the island densities at 180 K are relatively low, the scale of the STM images in Fig. 2c and d is relatively large (440 × 365 nm^2) and exceeds the terrace width. The rows of C_{60} islands seen in these images correspond to the atomic steps decorated by C_{60} islands. For evaluation of the island densities, these island rows and the denuded zones around the steps were excluded and only the islands located in the central part of the terraces were taken into consideration.

Double-logarithmic plots of island density versus C_{60} deposition rate for the two temperatures are shown in Fig. 2e. The fit yields the exponents $\chi = i/(i + 2)$ of (0.28 ± 0.02) at 109 K and of (0.31 ± 0.07) at 180 K. Both values are reasonably consistent with $i = 1$ in which ideal case the exponent χ would be 1/3. Note that the experimental values smaller than 1/3 are in fact typical. According to the rate equation theory, the exponent of 1/3 should be truly seen only in the limit of $D/R \to \infty$. As critical cluster is monomer, $E_i = 0$ and one readily obtains the diffusion barrier E_{diff}, which appears to be 99 meV for the "cold" surface and 370 meV for the "hot" surface. Note that this is a very unusual case, as typically the critical cluster size can grow with temperature while diffusion barrier remains the same (e.g., as for Cu on Ni(100) [4] or Fe on Fe(100) [45,5]).

A reasonable guess to account for the changeover of C_{60} diffusion mechanism at a critical temperature of ~150 K is to associate it with the presence of 2D gas of In adatoms, the peculiar feature of the (Au,In)/Si(111) surface. Mobility of In adatoms is believed to be lower than that of C_{60} (e.g., at 110 K, In adatoms are almost immobile, while

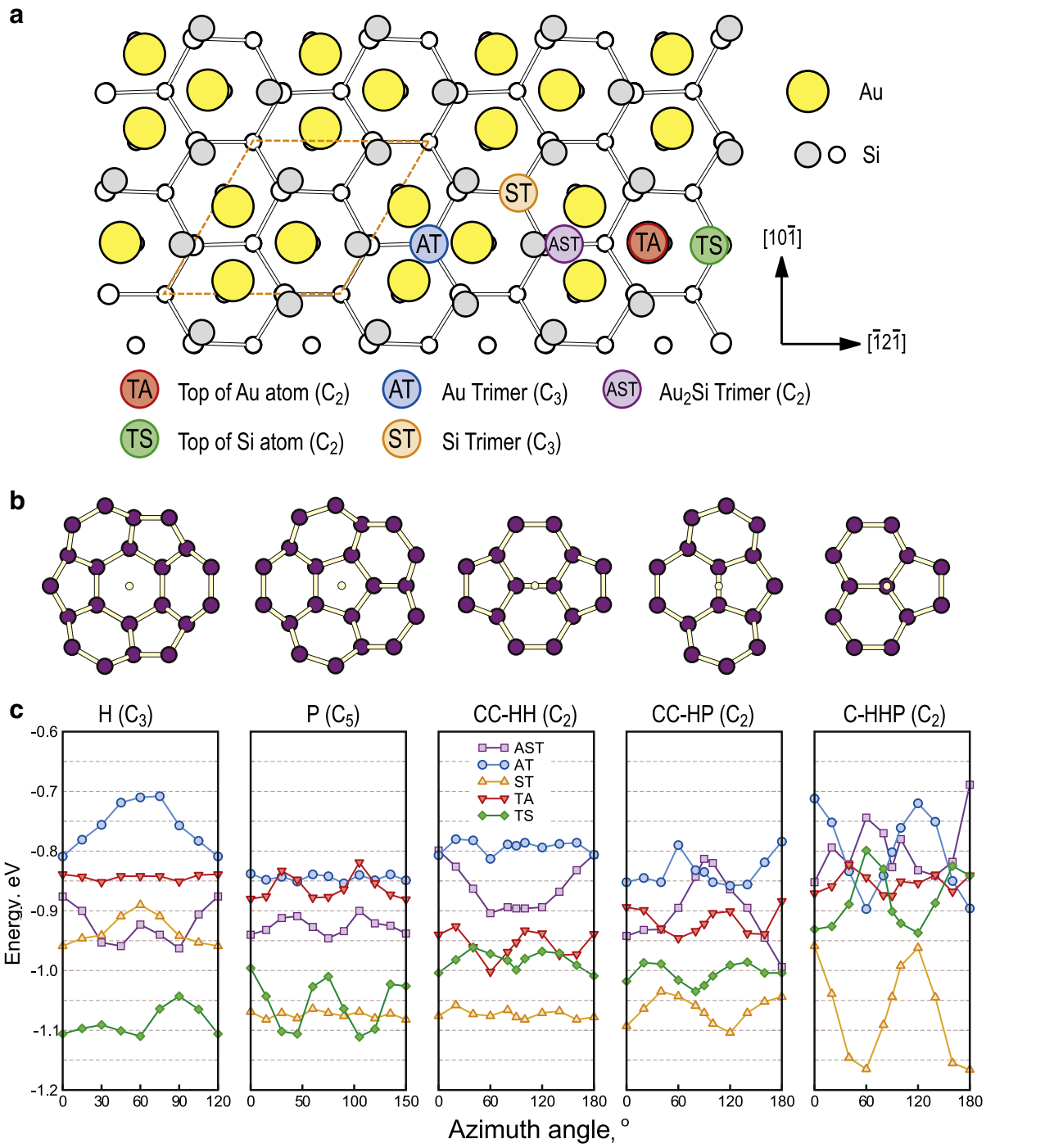

Fig. 4. Calculated bonding configurations of C_{60} on the In-free Si(111)$\sqrt{3} \times \sqrt{3}$-Au surface. (a) CHCT model of the surface with high-symmetry adsorption sites indicated. Symmetry groups of the corresponding sites are given in brackets together with the legend. Au atoms are shown by yellow circles, top Si atoms by gray circles, and Si atoms of the deeper layers by white circles. (b) Basic C_{60} orientations of C_{60} molecules at zero azimuthal angle. Location of the azimuthal rotation axis is indicated by open dot. Symmetry groups of the corresponding C_{60} orientations are given in brackets. (c) Azimuthal dependencies of C_{60} adsorption energy for various adsorption sites and basic orientations.

C_{60} molecules are still mobile enough to agglomerate into islands). Thus, diffusion of C_{60} on the surface is guided by a kind of labyrinth built of In adatoms like that shown in Fig. 3. One can assume that the diffusion barriers for C_{60} migration along the In rows are lower than those for crossing the rows. In this case, at low temperatures C_{60} motion would be confined by the labyrinth channels, while at high temperatures C_{60} would have enough thermal energy to surmount the labyrinth walls. Consequently, the one-dimensional-like migration at low temperatures changes for isotropic two-dimensional one at high temperatures. As a result, one would expect temperature dependence of diffusivity having two regions with different activation energies and pre-exponents, as observed in the present experiment. Note that this type of diffusion behavior is not very unexpected for such systems. For example, a similar result was reported for CO diffusion on Ni(110) where diffusion anisotropy along and across the atomic channels crosses over at a critical temperature [46,47].

To check the above assumption, we have conducted DFT calculations to characterize energetics of C_{60} diffusion in the labyrinth built of In atoms on Si(111)$\sqrt{3}\times\sqrt{3}$-Au surface. We have addressed first the adsorption geometries adopted by C_{60} molecules on the In-free Si(111)$\sqrt{3}\times\sqrt{3}$-Au surface (see Fig. 4). Five high-symmetry adsorption sites have been considered, including the top of Au atom (labeled TA), the top of Si atom (TS), the center of Au trimer (AT), the center of Si trimer (ST), and the center of Au_2Si trimer (AST), as shown in Fig. 4a. For each adsorption site, five basic C_{60} orientations have been checked, namely those having the following structural features at the C_{60} bottom close to the surface, hexagon (H), pentagon (P), C – C bond common to two hexagons (CC-HH), C – C bond common to hexagon and pentagon (CC-HP), and C atom common to two hexagons and one pentagon (C-HHP) (see Fig. 4b). Starting with the above basic configurations, the C_{60} molecules have been allowed to rotate around the normal to the surface which location is indicated in Fig. 4b by an open dot. The results of evaluation are presented in Fig. 4c which show the adsorption energies of C_{60} as a function of azimuth in various adsorption sites (given by five panels) and basic orientations (shown by plots of different colors). The C_{60} orientations corresponding to zero azimuthal angle are shown in Fig. 4b.

Table 1 shows the most stable C_{60} configurations occurring at Si(111)$\sqrt{3}\times\sqrt{3}$-Au surface as deduced from Fig. 4c. One can notice that different C_{60} orientations are preferable for various adsorption sites. The lowest energy configuration appears to be that of the C_{60} residing in the center of Si trimer (ST site) having C-HHP orientation rotated azimuthally by 60°. The next low-energy state having the close adsorption energy (only by 54 meV higher) corresponds to C_{60} residing atop Si atom (TS site) and having a pentagon at its bottom rotated by 105°. Occupation of the other three sites is noticeably less preferable.

Fig. 5 illustrates effect of In adatoms on the C_{60} adsorption onto Si(111)$\sqrt{3}\times\sqrt{3}$-Au surface. As an example, C_{60} occupying TS site with hexagon on the bottom (basic H orientation) is considered for the surfaces with one In and two In adatoms per $2\sqrt{3}\times2\sqrt{3}$ unit cell (corresponding to 1/12 and 1/6 ML In coverages, respectively) and compared with the In-free surface. Schematics in Fig. 5a illustrates the surfaces under consideration: In atoms reside in the ST sites [48]; In atoms shown by dark blue circles constitute 1/12 ML In coverage; In atoms shown by both light and dark blue circles constitute 1/6 ML In coverage. Fig. 5b presents the calculated azimuthal dependencies of adsorption energies for these three cases. One can see, that while the shape of the dependence plots is common for all cases, the plots go successively down with increasing In coverage. Thus, adding In atoms enhances C_{60} binding to Si(111)$\sqrt{3}\times\sqrt{3}$-Au surface in the TS site. The same trend is held for the AT and ST sites, the latter (i.e., the center of Si trimer) being the most energetically favorable site. In contrast, C_{60} occupation of the TA and AST sites becomes unstable in the presence of In atoms. It has been found also that placing In atom under C_{60} in a certain stable adsorption site (e.g., TS) results in weakening the binding by about 1.0 eV.

The next step is to consider the barriers for C_{60} migration on the In-free and In-accumulated Si(111)$\sqrt{3}\times\sqrt{3}$-Au surfaces. Schematics in Fig. 6a shows the principal pathways for C_{60} diffusion on the In-free surface, including that around the Au trimer (A–B–C) and across it (A–D), on the surface with 1/12 ML In (A′–B′–C′), on the surface with 1/6 ML In along the In atom row (A″–B″–C″) and on the same surface crossing the row in between two In atoms (A″–E). In the calculations, C_{60} molecule has been allowed to rotate during its motion along the pathway, and it has been found that molecule rolling is typically more efficient (i.e., is characterized by lower barriers) than a simple translation of C_{60} fixed in a given orientation. The barriers shown in Fig. 6b, c and d correspond to the optimal motions involving rolling [49]. In particular, Fig. 6b summarizes the calculation results for the pathway around Au trimer for the In-free surface and the surfaces with 1/12 and 1/6 ML In. On the In-free surface, the pathway (A–B–C) contains two barriers, 0.031 and 0.059 eV. These barriers are noticeably lower than that for the pathway (A–D) across Au trimer, 0.235 eV (Fig. 6c). When In atoms are added to the surface, the barrier for rolling around Au trimer increases to 0.193 and 0.243 eV for 1/12 and 1/6 ML In, respectively (Fig. 6b). The plausible reason is that the molecule has to visit energetically unfavorable sites B′ or B″ close to In adatom. However, the highest barrier of 0.773 eV is that for the pathway (A″–E) across the In row (Fig. 6d) as C_{60} approaches In adatoms there still closer. Calculations reveal that on this way C_{60} molecule even shifts In adatoms aside from their original locations [49].

Thus, the most principal results of calculations are as follows. Indium atoms have been found to retard migration of C_{60} on the Si(111)$\sqrt{3}\times\sqrt{3}$-Au surface as evidenced by increasing diffusion barriers. At In-accumulated surface, the diffusion barrier for C_{60} migration along In atom rows (i.e., within the labyrinth channel) is ~3–4 times lower than that for crossing In row (i.e., surmounting the labyrinth wall). This is

Table 1
Lowest C_{60} states for five different adsorption sites on the Si(111)$\sqrt{3}\times\sqrt{3}$-Au surface (CHCT model).

	AST	AT	ST	TA	TS
C_{60} orientation	CC-HP	C-HHP	C-HHP	CC-HH	P
C_{60} azimuth angle, °	180	90	60	60	105
Relative energy, eV	0.171	0.268	0.000	0.163	0.054

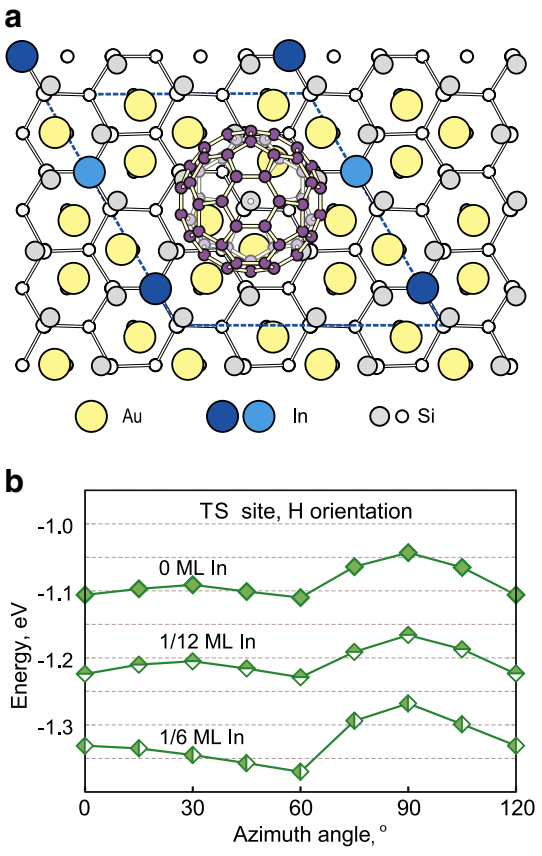

Fig. 5. Effect of In adatoms on the C_{60} adsorption energy. (a) Schematics showing the model structure for C_{60} residing atop Si atom (TS site) with hexagon facing the surface. Au atoms are shown by yellow circles, Si atoms by open circles, In atoms by blue circles. The $2\sqrt{3}\times\sqrt{3}$ cell is outlined. To describe the surface with 1/12 ML In, only In atoms shown by dark blue circles are taken into account. For description of the surface with 1/6 ML of In, In atoms shown by both dark and light blue circles are taken into account. (b) Azimuthal dependencies of adsorption energies for C_{60} in the TS site and H orientation for In-free Si(111)$\sqrt{3}\times\sqrt{3}$-Au surface and those with 1/12 and 1/6 ML In.

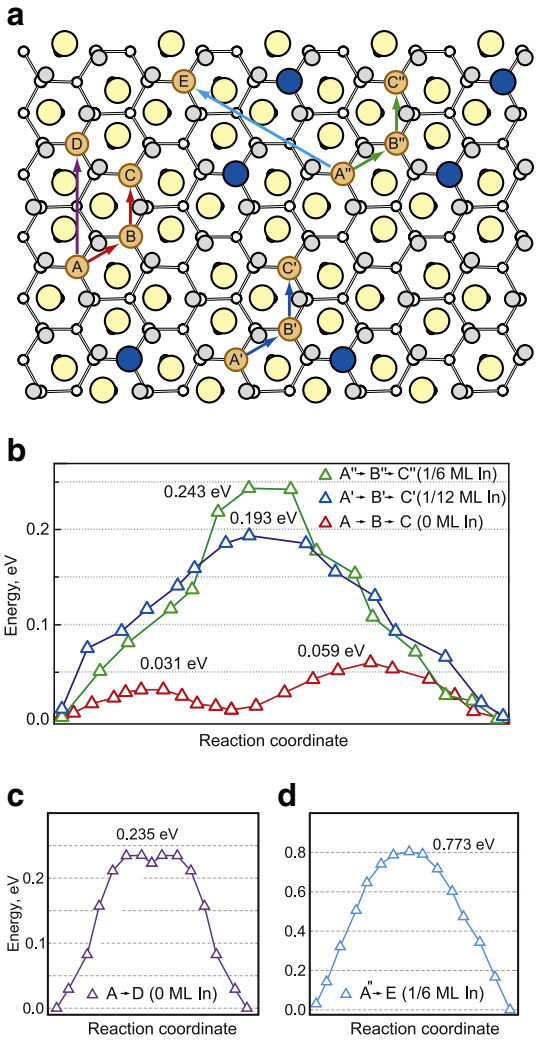

Fig. 6. (a) Schematics illustrating the principal pathways for C_{60} migration on the In-free Si(111)$\sqrt{3} \times \sqrt{3}$-Au surface and the surface with 1/12 and 1/6 ML In (for details see the text). Au atoms are shown by yellow circles, Si atoms by gray and white circles, and In atoms by blue circles. (b) Diffusion barriers for C_{60} migration around Au trimer on the In-free surface (the A–B–C pathway) and the surfaces with 1/12 (the A′–B′–C′ pathway) and 1/6 ML In (the A″–B″–C″ pathway). (c) Diffusion barriers for C_{60} migration across Au trimer on the In-free surface (the A–D pathway). (d) Diffusion barriers for C_{60} migration across In atom row on the surface with 1/6 ML In (the A″–E pathway).

consistent with the experimental results and may serve an argument supporting the above explanation of the occurrence of the two diffusion regimes.

As a final remark, we would like to note that though calculations demonstrate a qualitative resemblance with the experiment, the calculated barriers are approximately twice greater than those determined in the experiment. The possible reasons of the inconsistency are that the vdW-DF2 underestimates the interaction between C_{60} and metal atoms. For energy barrier calculations in this work, all the initial and final states are C_{60} on Si-rich ST sites; and the intermediate states are Au-rich AT site (e.g. A–D) or In-around sites (e.g. A″–E). Although the vdW-DF2 functional has been successfully tested for several organic molecules [42,50] and noble gases on metal surface [51], however, a recent study [52] reveals that the vdW-DF2 tends to underestimate the adsorption energy of C_{60} on Au(111). The underestimation of intermediate state energy has led to the overestimation of the reaction energy barrier. Several improvement methods are proposed and are in the development stage, such as vdW-DF2^{C09} [53] and PBE + vdW^{surf} [54,55], to more precisely describe the vdW forces of organics/metal surface system. The use of these new functionals might give more accurate values compared with experiment, but in this work the vdW-DF2 method has sufficiently given a qualitative resemblance for a description of C_{60} on In-free and In-accumulated Si(111)$\sqrt{3} \times \sqrt{3}$-Au surface.

4. Conclusion

In summary, we have studied diffusion of C_{60} molecules on the In-accumulated Au/Si(111) surface which comprises a highly-ordered homogeneous Si(111)$\sqrt{3} \times \sqrt{3}$-Au reconstruction with a 2D gas of In adatoms on it. For the determination of the diffusion parameters we have analyzed C_{60} island density as a function of growth temperature and C_{60} deposition rate in the framework of the rate equation theory. We have determined that a critical island size $i = 1$ is the same in the whole temperature range studied, from 110 to 240 K, while diffusion barrier varies from (99 ± 18) meV at 110 ÷ 140 K to (370 ± 24) meV at 160 ÷ 240 K. This finding has been accounted to the peculiarity of C_{60} migration in a labyrinth built of In adatoms, namely, at low temperatures C_{60} migration is confined within the labyrinth channels, while at high temperatures C_{60} molecules possess enough thermal energy to surmount the labyrinth walls. The results of the DFT calculations on C_{60} migration on In-free and In-accumulated Au/Si(111) sound supportive for the proposed mechanism of C_{60} diffusion on In-covered Si(111)$\sqrt{3} \times \sqrt{3}$-Au surface.

Acknowledgments

Part of this work was supported by the Russian Foundation for Basic Research (Grant Nos. 11-02-98516, 12-02-00430, 13-02-00837 and 12-02-31832), the Ministry of Education and Science of the Russian Federation (Grant Nos. 8022, 8581 and 2.1004.2011) and NSh-774.2012.2.

Appendix A. Supplementary data

Supplementary data to this article can be found online at http://dx.doi.org/10.1016/j.susc.2013.05.011.

References

[1] J.A. Venables, G.D.T. Spiller, M. Hanbücken, Rep. Prog. Phys. 47 (1984) 399.
[2] M. Bott, M. Hohage, M. Morgenstern, Th. Michely, G. Comsa, Phys. Rev. Lett. 76 (1996) 1304.
[3] Y.W. Mo, J. Kleiner, M.B. Webb, M.G. Lagally, Surf. Sci. 268 (1992) 275.
[4] B. Müller, L. Nedelmann, B. Fischer, H. Brune, K. Kern, Phys. Rev. B 54 (1996) 17858.
[5] J.A. Stroscio, D.T. Pierce, R.A. Dragoset, Phys. Rev. Lett. 70 (1993) 3615.
[6] H. Brune, G.S. Bales, J. Jacobsen, C. Boragno, K. Kern, Phys. Rev. B 60 (1999) 5991.
[7] A. Belianinov, B. Ünal, K.M. Ho, C.Z. Wang, J.W. Evans, M.C. Tringides, P.A. Thiel, J. Phys. Condens. Matter 23 (2011) 265002.
[8] A. Zangwill, D.D. Vvedensky, Nano Lett. 11 (2011) 2092.
[9] M. Einax, S. Ziehm, W. Dieterich, Ph. Maass, Phys. Rev. Lett. 99 (2007) 016106.
[10] M. Einax, W. Dieterich, Ph. Maass, J. Appl. Phys. 105 (2009) 054312.
[11] L. Sánchez, R. Ortega, J. Maria Gallego, R. Miranda, N. Martin, Chem. Rev. 109 (2009) 2081.
[12] L. Tang, X. Zhang, Q. Guo, Y.-N. Wu, L.-L. Wang, H.-P. Cheng, Phys. Rev. B 82 (2010) 125414.
[13] X. Zhang, L. Tang, Q. Guo, J. Phys. Chem. C 114 (2010) 6433.
[14] F. Loske, J. Lübbe, J. Schütte, M. Reichling, A. Kühnle, Phys. Rev. B 82 (2010) 155428.
[15] M. Körner, F. Loske, M. Einax, A. Kühnle, M. Reichling, Ph. Maass, Phys. Rev. Lett. 107 (2011) 016101.
[16] K. Aït-Mansour, P. Ruffieux, P. Gröning, R. Fasel, O. Gröning, J. Phys. Chem. C 113 (2009) 5292.
[17] A.V. Matetskiy, D.V. Gruznev, A.V. Zotov, A.A. Saranin, Phys. Rev. B 83 (2011) 195421.
[18] S. Korte, K. Romanyuk, B. Schiltzler, V. Cherepanov, B. Voigtländer, Phys. Rev. Lett. 108 (2012) 116101.
[19] F. Loske, M. Reichling, A. Kühnle, Jpn. J. Appl. Phys. 50 (2011) 08LB07.
[20] K.J. Franke, G. Schulze, N. Henningsen, I. Fernández-Torrente, J.I. Pascual, S. Zarwell, K. Rück-Braun, M. Cobian, N. Lorente, Phys. Rev. Lett. 100 (2008) 036807.
[21] D. Xu, E. Zhu, C. Lu, Y. Liu, Zh. Liu, D. Yul, J. He, Y. Tian, Appl. Phys. Lett. 96 (2010) 143115.
[22] J. Weckesser, J.V. Barth, K. Kern, Phys. Rev. B 64 (2001) 161403.

[23] S.H. Chang, I.S. Hwang, C.K. Fang, T.T. Tsong, Phys. Rev. B 77 (2008) 155421.
[24] D.V. Gruznev, I.N. Filippov, D.A. Olyanich, D.N. Chubenko, I.A. Kuyanov, A.A. Saranin, A.V. Zotov, V.G. Lifshits, Phys. Rev. B 73 (2006) 115335.
[25] T. Nagao, S. Hasegawa, K. Tsuchie, S. Ino, C. Voges, G. Klos, H. Pfnür, M. Henzler, Phys. Rev. B 57 (1998) 10100.
[26] J.K. Kim, K.S. Kim, J.L. McChesney, E. Rotenberg, H.N. Hwang, C.C. Hwang, H.W. Yeom, Phys. Rev. B 80 (2009) 075312.
[27] L.V. Bondarenko, D.V. Gruznev, A.A. Yakovlev, A.Y. Tupchaya, D. Usachov, O. Vilkov, A. Fedorov, D.V. Vyalikh, S.V. Eremeev, E.V. Chulkov, A.V. Zotov, A.A. Saranin, Sci. Rep. 3 (2013) 1826.
[28] D.A. Tsukanov, M.V. Ryzhkova, E.A. Borisenko, L.V. Bondarenko, A.V. Matetskiy, D.V. Gruznev, A.V. Zotov, A.A. Saranin, J. Appl. Phys. 110 (2011) 093704.
[29] Y.G. Ding, C.T. Chan, K.M. Ho, Surf. Sci. 275 (1992) L691.
[30] I.H. Hong, D.K. Liao, Y.C. Chou, C.M. Wei, S.Y. Tong, Phys. Rev. B 54 (1996) 4762.
[31] J.Y. Lee, M.H. Kang, J. Korean Phys. Soc. 55 (2009) 2460.
[32] G. Kresse, J. Hafner, Phys. Rev. B 47 (1993) 558.
[33] G. Kresse, J. Furthmüller, Comput. Mater. Sci. 6 (1996) 15.
[34] G. Kresse, D. Joubert, Phys. Rev. B 59 (1999) 1758.
[35] D.M. Ceperley, B.J. Alder, Phys. Rev. Lett. 45 (1980) 566.
[36] J.P. Perdew, K. Burke, M. Ernzerhof, Phys. Rev. Lett. 77 (1996) 3865.
[37] X. Lu, M. Grobis, K.H. Khoo, S.G. Louie, M.F. Crommie, Phys. Rev. B 70 (2004) 115418.
[38] L.-L. Wang, H.-P. Cheng, Phys. Rev. B 69 (2004) 165417.
[39] H.I. Li, K. Pussi, K.J. Hanna, L.-L. Wang, D.D. Johnson, H.-P. Cheng, H. Shin, S. Curtarolo, W. Moritz, J.A. Smerdon, R. McGrath, R.D. Diehl, Phys. Rev. Lett. 103 (2009) 056101.
[40] P.D. Godwin, S.D. Kenny, R. Smith, J. Belbruno, Surf. Sci. 490 (2001) 409.
[41] M. Dion, H. Rydberg, E. Schröder, D.C. Langreth, B.I. Lundqvist, Phys. Rev. Lett. 92 (2004) 246401.
[42] K. Lee, E.D. Murray, L. Kong, B.I. Lundqvist, D.C. Langreth, Phys. Rev. B 82 (2010) 081101.
[43] J. Klimes, D.R. Bowler, A. Michaelides, Phys. Rev. B 83 (2011) 195131.
[44] G. Mills, H. Jonsson, G.K. Schenter, Surf. Sci. 324 (1995) 305.
[45] J.G. Amar, F. Family, P.-M. Lam, Phys. Rev. B 50 (1994) 8781.
[46] X.-D. Xiao, X.D. Zhu, W. Daum, Y.R. Shen, Phys. Rev. Lett. 66 (1991) 2352.
[47] X.-D. Xiao, X.D. Zhu, W. Daum, Y.R. Shen, Phys. Rev. B 46 (1992) 9732.
[48] H.W. Yeom, T. Abukawa, M. Nakamura, X. Chen, S. Suzuki, Surf. Sci. 340 (1995) L983.
[49] See Supplemental Material for details of C_{60} motion along the pathways.
[50] K. Müller, A.P. Seitsonen, T. Brugger, J. Westover, T. Greber, T. Jung, A. Kara, J. Phys. Chem. C 116 (2012) 23465.
[51] D.-L. Chen, W.A. Al-Saidi, J.K. Johnson, J. Phys. Condens. Matter 24 (2012) 424211.
[52] I. Hamada, M. Tsukada, Phys. Rev. B 83 (2011) 245437.
[53] V.R. Cooper, Phys. Rev. B 81 (2010) 161104.
[54] V.G. Ruiz, W. Liu, E. Zojer, M. Scheffler, A. Tkatchenko, Phys. Rev. Lett. 108 (2012) 146103.
[55] W. Liu, J. Carrasco, B. Santra, A. Michaelides, M. Scheffler, A. Tkatchenko, Phys. Rev. B 86 (2012) 245405.